Crosswell seismic applications to highly heterogeneous tight gas reservoirs

Peter C. Leary[1*] and Larry A. Walter[1]

The nature of geological heterogeneity is well understood in proximity to a wellbore but is sparsely sampled laterally. Heterogeneity is both highly unpredictable and difficult to map with surface reflection seismics, but high productivity trends in tight gas reservoirs can be efficiently identified with precision crosswell seismic time-lapse travel-time data.

Geophysical v geological heterogeneity

It is well known that accurate geological reservoir models do not lead often to accurate fluid flow predictions, either near or far from reservoir wells. The failure of geological reservoir models to accurately predict reservoir flow is due to the common but unwarranted assumption that geological facies have uniform porosity and permeability fixed by sampling at wellbore scales. Such upscaling of sparsely sampled wellbore data is especially unwarranted in light of evidence for fracture-density fluctuations that systematically affect porosity and permeability at scale lengths from mm (grains) to km (the reservoir itself). Low porosity, low permeability tight gas reservoirs drained by fracture-dominated flow paths are especially sensitive to spatially erratic fracture heterogeneity.

Efficient tight gas production favours siting infill wells in fracture-rich rather than fracture-poor reservoir volumes. Conventional reflection seismic imaging is unlikely to distinguish between the two. Aiming to identify fracture rich trends in tight gas fields, we simulate time-lapse crosswell seismic travel-time data for realistic models of reservoir fracture heterogeneity based on the fracture phenomenology latent in well-log data.

In situ fracture heterogeneity

Well-log and well-core geophysical data reveal a robust picture of heterogeneity closely tied to *in situ* fractures. A summary of essential aspects of well log and well core data is:

(i) Well log spatial fluctuation power spectra scale inversely with spatial frequency k, $S(k) \propto 1/k$, over scale lengths of mm to km.

(ii) The spectral trend $S(k) \propto 1/k$ of most geophysical logs (sonic velocity, mass density, neutron porosity, gamma activity, chemical abundance, electrical resistivity) is plausibly due to spatial fluctuations in the density of grain-scale percolation fractures.

(iii) Spectral trend $S(k) \propto 1/k$ shows that geophysical fluctuations are spatially correlated at all scales from mm to km (spatially uncorrelated fluctuations, denoted by flat power spectra $S(k) \propto const$, are necessary for reliably predicting reservoir-scale properties from well bore sample properties).

(iv) Clastic reservoir well core porosity and log (permeability) spatial fluctuations are 80-85% correlated, $\delta\varphi \approx \delta\log(\kappa)$.

(v) Well core poroperm fluctuation relation $\delta\varphi \approx \delta\log(\kappa)$ mathematically links grain-scale fractures to fluid percolation via fracture density if $\delta\varphi \propto \delta n$, n the number of fractures per unit volume, and permeability is proportional to fracture percolation pathway combinatorics, $\kappa \propto n!$; Stirling's formula reduces $\delta\log(n!)$ to the mathematical relation $\delta\varphi \approx \delta\log(\kappa)$.

The spatial correlation of geophysical fluctuations identified by well log spectra $S(k) \propto 1/k$ formally invalidates the practice of predictively completing reservoir geological models with quasi-uniform porosity and permeability values from well bore data. This formal invalidity makes a *prima facie* case that typical reservoir model flow predictions fail because of incorrect statistical treatment of geophysical heterogeneity. If well bore reservoir sampling data are insufficient for accurate predictive reservoir models, new data are needed. Oil field practice increasingly *de facto* recognizes this argument by investing in observation of reservoir scale flow structures using time-lapse seismic snapshots of reservoir flow. We apply a detailed form of this general argument to tight gas production by (1) explicitly describing the reservoir in terms of *in situ* fracture density fluctuations and (2) mapping reservoir scale fracture heterogeneity by using simulated crosswell seismic travel-time monitoring to locate zones of rapidly depleting gas pressure.

A tight gas reservoir model

Fig 1 illustrates a generic 2D reservoir model section based on the spatially correlated *in situ* fluctuation properties observed in well logs and well core. The spatial fluctuations in Fig 1 embody the above physical features (i)-(v) with a few additional assumptions. Each point represents fracture

[1] *Geospace Engineering Resources International, 7007 Pinemont Drive Houston TX 77040, USA.*
[*] *Corresponding author, E-mail: pcleary1@blueyonder.co.uk.*

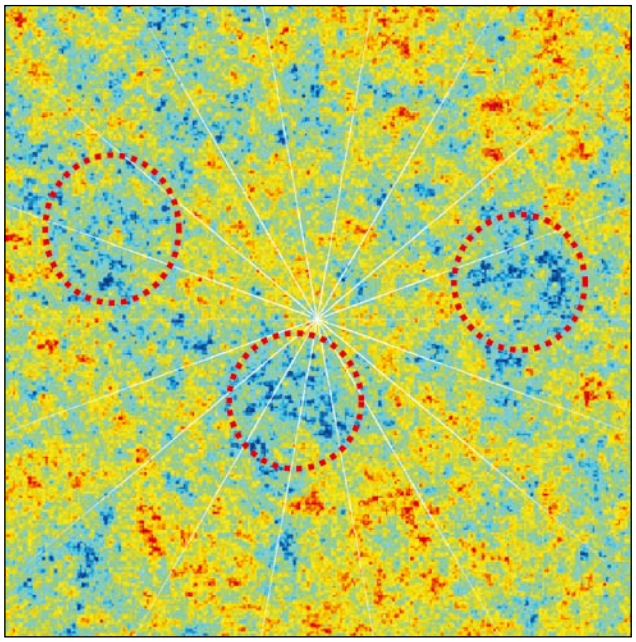

Figure 1 *Spatially correlated random noise fracture density distribution with frequency dependent power spectrum S(k) ≈ 1/k. Cool colours = higher fracture density, warm colours = lower fracture density. White lines mark azimuthal sectors about a central well. Red circles mark zones of rapid well pressure depletion due to high fracture density and fracture connectivity.*

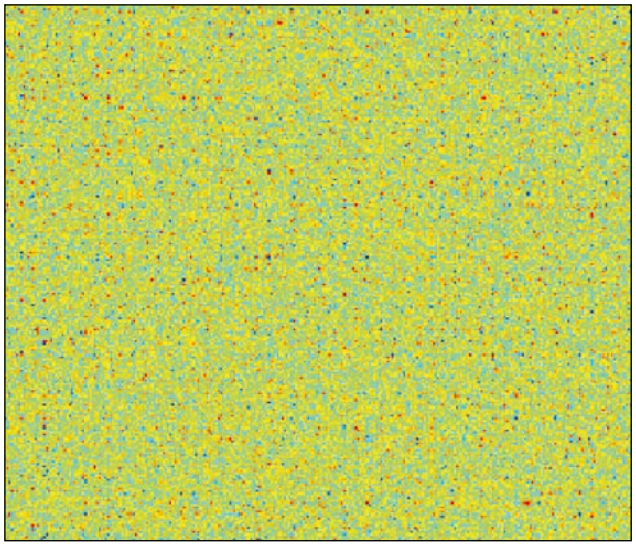

Figure 2 *Spatially uncorrelated random noise with frequency independent power spectrum S(k) ≈ const. The variance of Fig 2 fluctuations is the same as the variance of Fig 1 fluctuations.*

density n = number of grain-scale fractures per unit volume, with fracture density fluctuations δn spatially correlated according to power-spectrum $S(k) \propto 1/k$, and reservoir permeability related to fracture density by $\delta n \approx \delta \log(n!)$. Additional assumptions are:

1. The 2D reservoir section originates as a slice of a 3D volume; 3D fluctuations are, however, assumed negligible at short distances normal to the section.
2. Fracture density fluctuations δn are physically/spatially correlated with fluctuations in acoustic velocity, $\delta\alpha \propto -\delta n$.
3. The reservoir has a single fluid phase.
4. Acoustic velocity variation is related to fluid pressure variation as $\delta\alpha \approx G\delta P$, where G is empirically given as $(d\alpha/\alpha)/dP \approx 1/6$GPa.

To contrast the spatially erratic reservoir section of Fig 1, Fig 2 illustrates a reservoir section based on uncorrelated spatial fluctuations. All other features of the Fig 2 reservoir model remain the same as the Fig 1 model. Visual inspection of Figs 1 and 2 shows the fundamental statistical difference between correlated and uncorrelated spatial fluctuations. While it is visually plausible that small-scale sampling of a Fig 2 spatially uncorrelated section fixes fluctuations at all other scales (i.e, $S(k) \propto const$), small-scale sampling of the Fig 1 spatially correlated section clearly does not constrain spatial fluctuations elsewhere in the section.

Fracture density as the basis of flow heterogeneity in crustal reservoirs

Figs 3 and 4 illustrate well log spectral data and North Sea clastic well core poroperm data that underwrite the Fig 1 spatial heterogeneity model. Figs 5 and 6 then calibrate the Figs 1 and 2 heterogeneity models by comparing flow heterogeneity statistics observed in tight gas well production data from western Colorado (Fig 5) with fluid flow simulation statistics for spatially correlated and spatially uncorrelated porosity heterogeneity (Fig 6).

Fig 3 shows well-log spectra in log-log form from three geological settings. Power-law fluctuations of each spectrum are fit to a straight line in the log-log domain to yield a power-law exponent β as in spectral form $S(k) \propto 1/k^{\beta}$. The mean value of the Fig 1 sample spectra is 1.08 ± 0.17. A sample of several hundred power-law spectra has mean value 1.02 ± 0.1 (Leary 2002; cf. Goff & Holliger 2002).

Site	Wells	Samples	Total Z (m)	Mean ΔZ (cm)	Mean χ(%)
Germany	13	2459	421	17	88±8
North Sea	16	2334	880	37	85±5

Table 1 *Well-core poroperm data profiles for data illustrated in Fig 4. The reservoir sites are, respectively, onshore and offshore gas fields. Each of the 13+16 well core sections produced a porosity and log (permeability) sequence; for each sequence the mean was removed, the sequence normalized by its variance, and the resulting sequence pair cross-correlated to give coefficient -100% < χ <100%. The table gives the mean and standard deviation of the individual coefficients. Fig 4 overlays sample reduced porosity and log (permeability) sequences. Data are courtesy of Roberto Peveraro.*

Power-law spectra $S(k) \propto 1/k^{\beta}$, $\beta \sim 1$, indicate a physical process without a fundamental scale length. Such processes are well known in certain thermodynamic systems close to a critical-state phase transition. Long range spatial correlations and power-law scaling spatial fluctuation spectra characterize permanent magnets, water at its triple point, and critically opalescent binary fluids. If we take grain-scale fracture density as a thermodynamic variable, the thermodynamic critical state serves as a reference system for crustal rock. Associating fracture density with fluid percolation, we can use *in situ* critical-state percolation network phenomena as a physical analogue to critical state thermodynamic systems (Binney et al. 1995; Stauffer and Aharony 1994; Leary 1997).

The empirical link $\delta\varphi \approx \delta\log(\kappa)$ between fracture density and permeability completes the physical model by directly associating fracture density with percolation networks. An 80% spatial correlation for poroperm relation $\delta\varphi \approx \delta\log(\kappa)$ was reported by Leary and Al-Kindy (2002) for 1600 samples from 750 m of core from four North Sea oil field wells. The link is strengthened by data illustrated in Fig 4 and summarized in Table 1. An 87±6% spatial correlation for $\delta\varphi \approx \delta\log(\kappa)$ is recorded for a sample of 4800 core plugs from 1300 m of clastic reservoir well core from 29 wells in two gas fields.

In Fig 4 each well core porosity sequence is plotted as a zero-mean unit-variance sequence. The same reduction performed on log (permeability) sequences is then overlain on the porosity sequence. The reduced sequence pairs are >80% cross-correlated, $\delta\varphi \approx \delta\log(\kappa)$. Highly correlated spatial fluctuations in porosity and log (permeability) imply a close physical relation between fracture density correlated with porosity and fracture connectivity correlated with permeability.

The expression $\delta\varphi \approx \delta\log(\kappa)$ can be derived from percolation fracture density expressed as the number n of grain-scale fractures per unit volume. Let fracture connectivity be a combinatorial phenomenon involving terms such as $n! = n\times(n\text{-}1)\times(n\text{-}1)\ldots2\times1$. Then $\delta\log(\kappa) \propto \delta\log(n!)$ reduces permeability fluctuations to the scale of fracture density fluctuations δn. For fracture density fluctuations $\delta n << n$, log(permeability) fluctuations are of order $\delta\log(\kappa) \propto \log((n+\delta n)!) - \log(n!)$, and by Stirling's formula, $\log(n!) \approx (n+1/2)\log(n) - n$ for $n >> 1$, permeability perturbations are $\delta\log(\kappa) \approx \delta n\, log(n)$. Since $log(n)$ is essentially constant, removing it by normalizing fluctuation sequences to unit variance gives $\delta\log(\kappa) \approx \delta n$ as in Fig 4 and Table 1.

Flow heterogeneity in tight gas reservoirs

Tight gas flow is thought to be dominated by fracture networks, while geological interfaces in tight gas formations are typically between similar sand/shale units rather than between units of strong geological contrast. We can test the Fig 1 model of geophysical heterogeneity by comparing the spatial fluctuations in well productivity observed in tight gas fields with model well productivity fluctuations based on Figs 1 and 2.

The degree of flow heterogeneity encountered in western Colorado gas fields is seen in the Fig 5 crossplot between the extent of gas-sand intervals in each well (Net-Pay) and the observed well production (EUR). According to

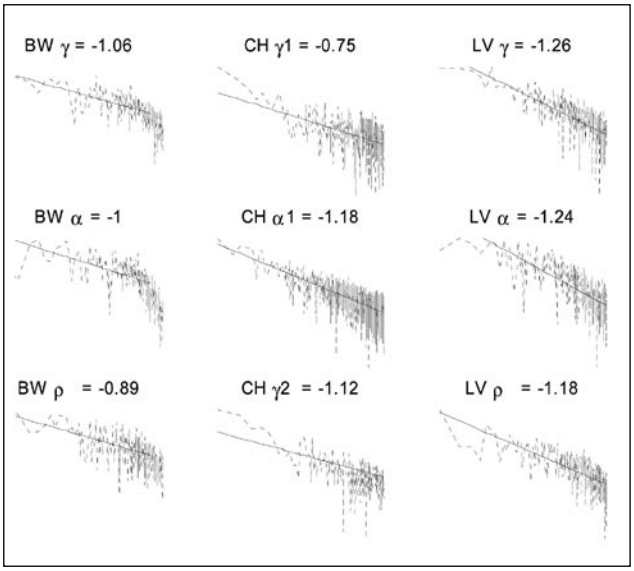

Figure 3 *Well log power spectra from 3 sites (BW=gas field, Germany; CH=tight gas sands, Colorado; LV=basement rock, California); γ = gamma activity; α = sonic velocity; ρ = mass density). Horizontal axes for each spectrum is spatial frequency; the minimum spatial frequency is 1/L(m), L(m) = the well log length in metres; the maximum spatial frequency is typically ½ m to 1/3 m, thus allowing for the finite length of the logging tool. Vertical axes for each spectrum is fluctuation power in arbitrary units. Sample mean power-law exponent is 1.08 ± 0.17; Leary (2002) summarizes several hundred well log spectral exponents having mean value 1.02 ± 0.1. In the CH log suite, two gamma activity sensors were deployed while a sonic velocity log was not acquired.*

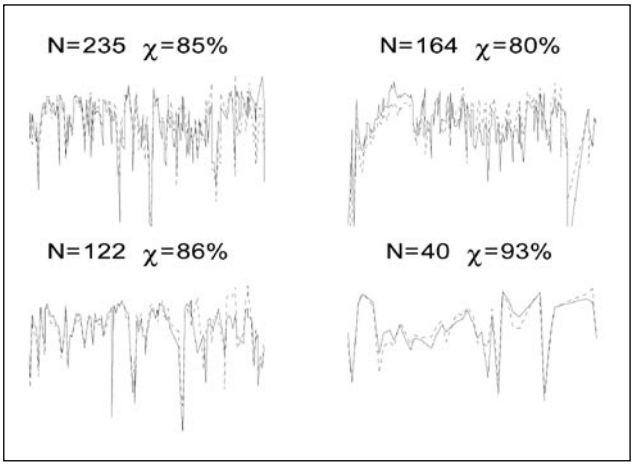

Figure 4 *Overlays of sample zero mean, unit variance well core poroperm sequences from North Sea clastic reservoir gas fields; N=number of well-core samples in poroperm sequence; χ=crosscorrelation coefficient. Horizontal axes of each plot are the core plug well depths. Vertical axes are the spatial fluctuation amplitude normalized to unit variance. Data are courtesy of Roberto Peveraro.*

the Fig 2 picture of spatially uncorrelated reservoir heterogeneity, gas production in a well (EUR=estimated ultimate recovery) is predictable by combining the extent of gas reservoir rock penetrated by a well (Net-Pay) with permeability estimated from well core or well log data. Fig 5 shows the expected EUR/Net-Pay correlation is clearly absent.

Figs 1, 3, and 4 imply that the broad scatter of Fig 5 data arises because Fig 2 is not a physically valid model of *in situ* fracture spatial correlation. Instead, tight gas well productivity is likely to be subject to Fig 1 spatial fluctuations in both storage and permeability on all scales, most particularly on scales that exceed the volume of individual geological reservoir units.

We quantify the effect on well productivity of Fig 1 spatially correlated fracture-density heterogeneity and associated reservoir permeability via the diffusion equation for heterogeneous media, $\partial_t P \propto \nabla\bullet(\kappa\nabla P)$. A number of wells can be supposed to be drilled through Figs 1-2 2D reservoir sections. With the reservoir sections initially at a uniform gas pressure, gas flows from the reservoir into a well in proportion to the local fracture density and fracture connectivity structures of the heterogeneous medium. The lower the gas pressure at a fixed interval in time, the more productive the well.

Fig 6 summarizes the results of flow simulations for spatially correlated Fig 1 heterogeneity and spatially uncorrelated Fig 2 heterogeneity. The upper plot 'x' distribution shows the well production scatter implied by Fig 1 heterogeneity, in generic agreement with the Fig 5 observed scatter.

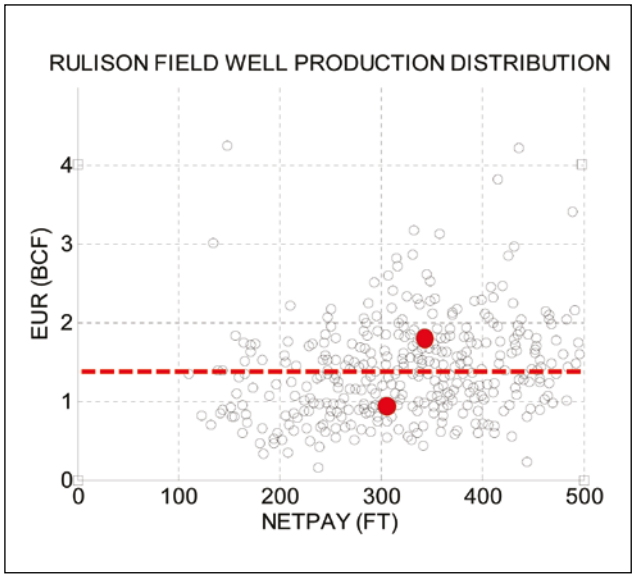

Figure 5 *Crossplot of expected well productivities (Net-Pay, measured in feet of gas-sand intersected by a well) and actual well productivities (EUR = estimated ultimate recovery in billions of cubic feet of gas based on short term production of each well). Red line marks median divide between good producers and poor producers; red dots mark median values of populations divided by red line. Data are from the Rulison gas field, western Colorado, courtesy of Steve Cumella.*

In contrast, the 'o' distribution in the upper plot shows the traditionally expected correlation for well production data has little agreement with observed data.

The lower plot of Fig 6 gives a different statistical comparison of Fig 5 data and Fig 1-2 spatial correlation types. Fig 5 and Fig 1 well production have broader scatter about the mean, in particular having tails towards larger values (standard deviation 50% of mean) while Fig 2 well production scatter remains relatively close to the mean (standard deviation 25% of mean). The higher degree of fluctuation relative to the mean and the longer statistical tails are diagnostic of spatially correlated fracture heterogeneity.

Multiple crosswell seismic time-lapse profiling

On the evidence of Figs 5 and 6, Fig 1 can represent a horizontal tight gas reservoir section of some physical dimension. Taking that dimension to be 2 km on a side, Fig 7 shows a grid of 40 acre production wells. The wells can intersect

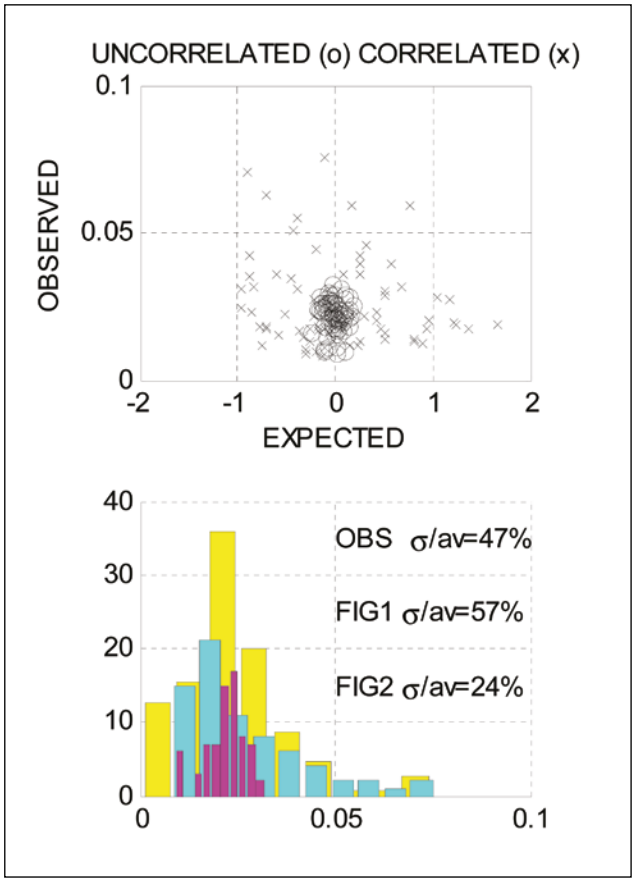

Figure 6 *(Upper) Synthetic crossplots of expected and observed well production: expected well production is given by the porosity and permeability immediately around the well; observed well production is given by the well pressure after a fixed interval of fluid diffusion; 'x' marks flow in Fig 1 heterogeneity; 'o' marks flow in Fig 2 heterogeneity. (Lower) Distribution about the mean of observed well production (yellow), Fig 1 heterogeneity simulation well production (cyan), and Fig 2 heterogeneity simulation well production (magenta); observed and Fig 1 distributions have longer tails than does the Fig 2 distribution as seen in the ratios of standard deviations to means.*

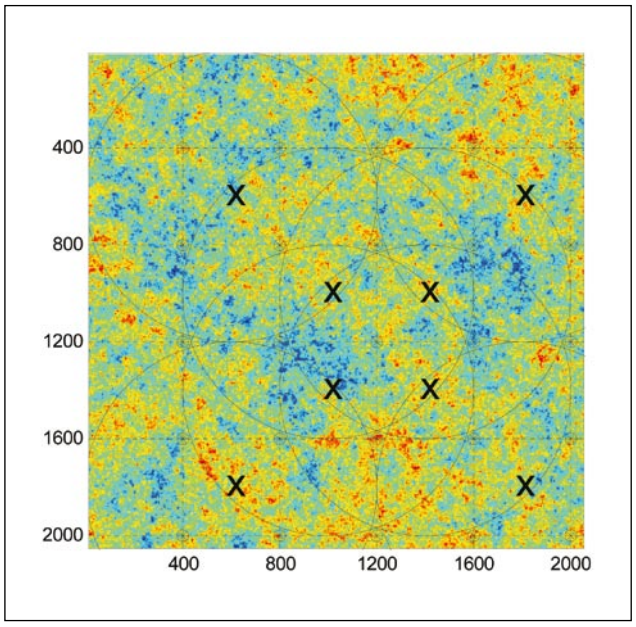

Figure 7 *Fig 1 spatially correlated noise interpreted as a fracture density map of a 2 km x 2 km horizontal section of a tight-gas production formation at depth. A 40 acre (400 m) grid of production wells denoted by solid dots is instrumented with seismic motion detectors. Source wells denoted by X emit seismic waves recorded at sensor wells to order 50 μs resolution. Travel-times in interwell sectors rich in fractures show marked time-lapse changes while travel-times in sectors poor in fractures remain unchanged.*

small-scale zones of high fracture density with good well productivity (cool colours) or small-scale zones of low fracture density with poor well productivity (warm colours). In principle, an infill drilling programme to 20 acre and 10 acre well spacing can be based on small-scale well productivity data alone (drill infill wells close to good producers), but Fig 5 indicates this principle is no better than, say, the usual practice of random infill drilling. Fig 7 shows why. An initially good producer may intersect only a relatively small zone fracture zone but not be a good long term producer. A better infill drilling strategy explicitly recognizes the Fig 1 spatial noise distributions are spatially correlated at all scale lengths and small-scale data cannot be reliably extended to larger scales. A broader survey of reservoir structure surrounding each well is needed.

Neither static nor time-lapse reflection seismics are likely to yield requisite cost effective spatial information over a reservoir layer such as Fig 1. Reflection images identify spatially uniform geological interfaces rather than spatially erratic fluctuations in layer fracture density. Time-lapse reflection seismic imaging focuses on time changing layer properties but image sensitivity is typically limited by unstable wavelets from surface sources and unstable response functions from redeployed surface sensors. Time-lapse reflection seismic surveys are also likely to be prohibitively expensive.

High precision multiple azimuth time-lapse crosswell seismic travel-time surveying is a much lower cost means

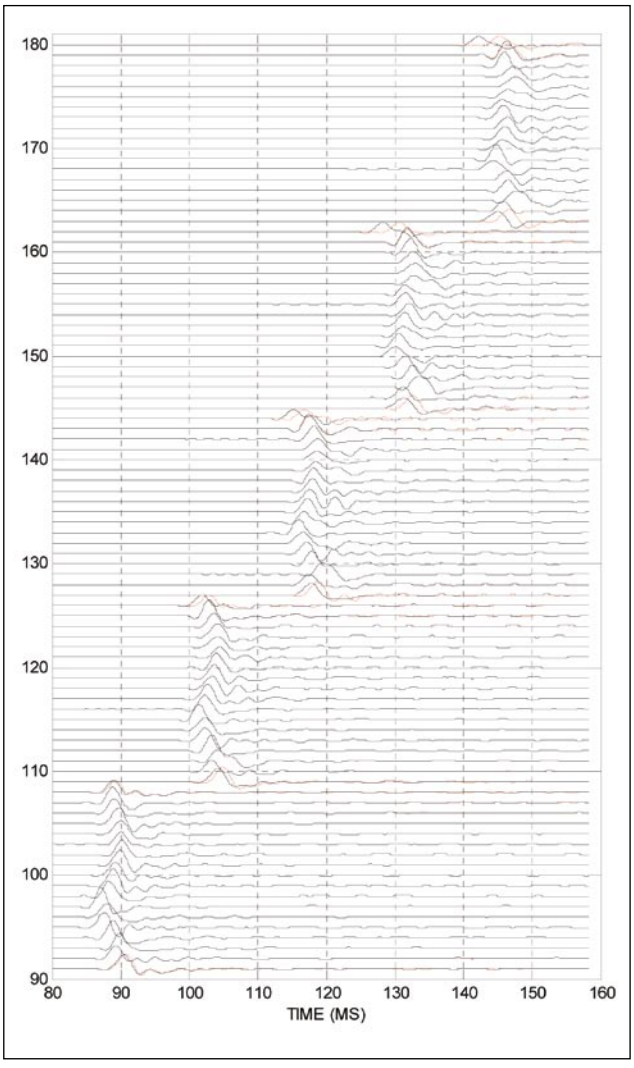

Figure 8 *Sample multiple azimuth time-lapse travel-time data at five radial offsets for a Fig 1 crosswell geometry of a central well within sensor well grid of 10 acre spacing (four times denser than Fig 7). Red traces indicate visually detectable time-lapse changes relative to black traces. Resampling traces by 100 allows trace cross-correlation to fix travel-time differences to 3 μs precision (beneath visual detection in this plot). Source waveform stability of ≈ 3 parts in 104 allows meaningful field data travel-time resolution of ≈100μs at 1 km offsets. In the data shown, large time-lapse changes are evident in the two sectors corresponding to the top and bottom trace at each radial offset; these azimuths are those of the red circle at 7 pm in Fig 1.*

of identifying reservoir sectors releasing stored gas through large scale high density fracture networks and hence becoming a target for infill drilling. Fig 7 shows the Fig 1 reservoir heterogeneity section with an initial set of production wells at 40 acre (400 m) well spacing. Each well (black dot) is completed with behind-the-casing seismic sensors at the reservoir section depth. A crosswell seismic source visits selected wells denoted by Xs in the centre of the sensor grid. Each source well is at the centre of a 600 m radius circle, showing that a source well can provide time-lapse travel-time sampling for 12 surrounding radial-azimuthal sectors (four azi-

muths at radius 400 m and eight azimuths at radius 565 m). At 1 km range, a borehole seismic source approximately doubles the radial/azimuth sensor count. As a downhole seismic source, the swept-frequency downhole orbital vibrator (DOV) has a 1 km range in competent reservoir rock and sufficient source wavelet stability for 50-100μs travel-time resolution over 300 ms travel paths (Leary and Walter 2005a,b; Leary et al. 2005).

Figs 8 and 9 illustrate the process of time-lapse crosswell seismic travel-time inversion for the simplest case of the single source well shown in Fig 1 with signals recorded at up to 1 km offsets. To illustrate the data inversion process more incisively, the well grid surrounding the single source is taken as 10 acre (200 m) spacing (four times greater than shown in Fig 7). Each sensor well extracts gas from the surrounding formation. At 1 km range, crosswell travel-times ≈300ms monitored to 50-100μs resolution gives time-lapse sensitivity of up $\approx 3/10^4$ for 150 radial-azimuthal sectors (18 equally spaced azimuths at eight approximately equally spaced radii). The 150 sectors shown in Fig 9 are sampled by time-lapse travel-time data recorded at ≈ 100 wells. Radial-azimuth sectoring of the sensor well grid enables a more stable linear inversion scheme, hence is simpler to implement than the more standard rectilinear grid scheme. Velocity pressure sensitivity $(d\alpha/\alpha)/dP \approx 1/6$GPa from time-lapse observations in the North Sea (Landro et al., 2005; Barkved and Kristiansen, 2005; Eiken and Tondel, 2005; Hofmann et al., 2005) gives reservoir model time- and space-dependent pressure/velocity changes in the Fig 1 fracture density distribution. Finite difference acoustic wave propagation across the Fig 1 fracture density/slowness grid yields time-lapse crosswell travel-time data for the ≈ 100 sensor wells. Fig 8 shows sample time-lapse seismograms for five radial offsets over the 18 azimuthal sectors. Red traces mark visually detectable wavelet travel-time changes for waves passing through sectors most affected by local well gas extraction (the two azimuths most affected are those in the red circle at approximately 7 pm in Fig 1).

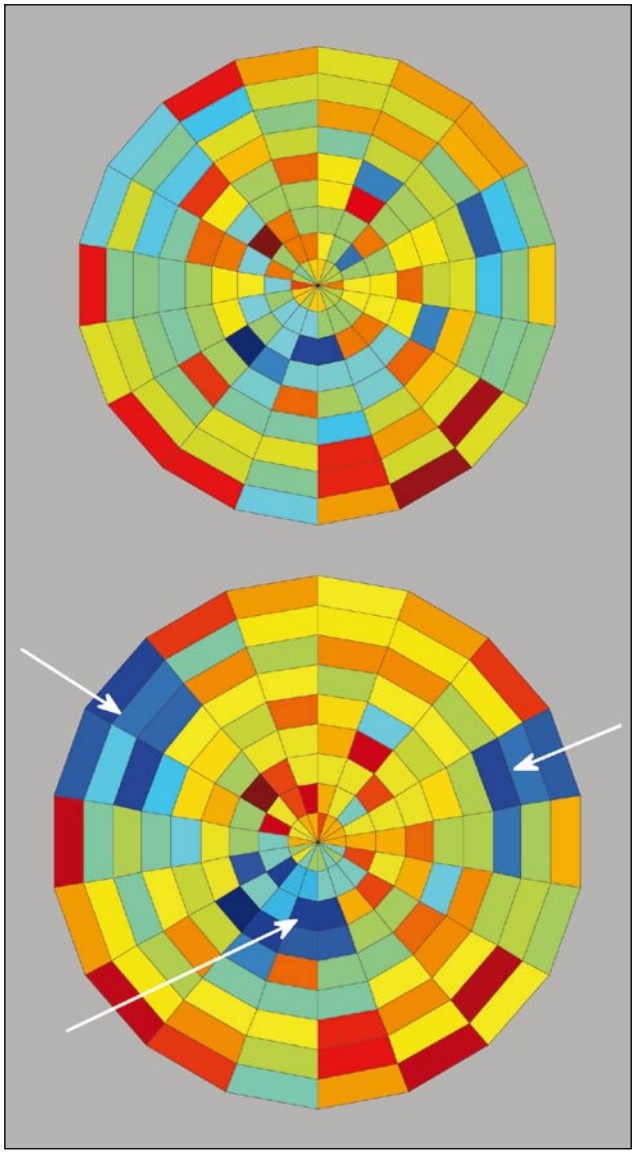

Figure 9 *Radial-azimuthal sector plot of time-lapse travel-time differences due to drawdown of Fig 1 reservoir section by a grid of 10 acre production well. Target high fracture density reservoir sections are circled in red in Fig 1 and noted by arrows in the lower sector plot. The two sector plots are the same everywhere except as noted by the arrows, where, as circled in Fig 1, the high permeability sections are most changed by rapid pressure loss due to high gas production.*

Fig 9 radial/azimuthal sector plots summarize travel-time inversion for the simulated time-lapse crosswell seismic travel-time survey sampled in Fig 8. The upper sector plot shows initial travel-times for 144 source sensor travel paths across the Fig 1 reservoir slowness field. The lower sector plot shows travel-time detection of pressure depletions due to gas production by the 10 acre production grid surrounding the single source well. Comparison of the two plots shows that the lower plot has three deep blue sectors noted by arrows. These positions correspond to the Fig 1 high fracture density areas of the fracture density field (areas of cool colours circled in red).

The Fig 9 time-lapse radial/azimuthal sector plots are produced by standard velocity tomography applied in polar coordinates. Velocity tomography computes grid slowness values by inverting the linearized travel-time expression $\mathbf{Ws} = \mathbf{t}$, where $\mathbf{t}$ is the vector of the $N_{rad}*N_{az}$ travel-times computed by finite differences between the central source and sensors on N_{az} azimuths at N_{rad} radii about the source of the Fig 1 slowness grid, $\mathbf{s}$ is the vector of the $N_{rad}*N_{az}$ (unknown) radial-azimuthal slownesses sectors of Fig 1, and $\mathbf{W}$ is the matrix of geometric weights giving the fraction of each straight line raypath spent in each radial-azimuthal sector. Here for a single source well N_{rad}= 8 outer radii and N_{az} = 18. Unlike the equivalent

matrix for standard crosswell velocity tomography on a rectilinear grid, the straight-line ray-weight matrix **W** for radial-azimuthal sectors has a stable inverse $\mathbf{W}^{-1}$, giving the vector of sector slownesses $\mathbf{s} \approx \mathbf{W}^{-1}\mathbf{t}$ without the complication of singular value decomposition of **W**. The simplicity and stability of the radial-azimuth sector inversion follows from the data acquisition geometry. Radial-azimuthal sector inversions using, say, 40 acre spacing for the sensor grid can be performed for multiple source wells. Data from the overlapping regions between sensor wells can be inverted using a globalized version of $\mathbf{Ws} = \mathbf{t}$ for multiple source wells or locally reconciled by weighted averaging of multiple overlapping single well estimates for 40 acre spacing slowness sectors.

Summary and conclusions

Figs 1-9 summarize (1) the problem posed to efficient tight gas production by the erratic and unpredictable nature of *in situ* fracture heterogeneity, and (2) a solution that exploits the tight gas field well geometry, number, and stability for downhole seismic sensing and sourcing to acquire highly sensitive time-lapse volumetric monitoring data to characterize the producing reservoir. Inverting systematically acquired time-lapse data can lead to rational siting of infill wells in the most fracture rich hence most productive reservoir sectors. The crosswell seismic solution to the tight gas reservoir fracture heterogeneity problem assumes (1) that each well is instrumented (presumably at completion) with seismic sensors throughout the reservoir depth, and (2) that ≈ 10% of wells are managed to allow temporary entry of a slimline borehole benign seismic source (such as the DOV) at suitable time intervals during reservoir development and production. It is also tacitly assumed that the 2D data acquisition simulated here for a single depth section is extended to 3D coverage of the reservoir by application over 30-50 m depth intervals.

If such a crosswell seismic monitoring programme is systematically carried out at all depths in a tight gas reservoir, and if Fig 1 heterogeneity is a physically realistic model for the scatter in the Fig 5 well production data, our modelling indicates that infill well siting can discriminate between, say, the 50% most productive well sites and the 50% least productive well sites. Fig 5 data indicate that median production from the poor producers is ½ BCF lower than the median while median production from the good producers is ½ BCF higher. In an ideal crosswell seismic monitoring scenario based on the production data of Fig 5, the estimated per well benefit of infill drilling only good producers is 1 BCF. The income for such improved reservoir production is likely to be very much greater than the median per well cost of crosswell seismic monitoring.

Acknowledgements

The clastic reservoir well core poroperm data of Fig 4 and Table 1 were contributed by Roberto Peveraro, Petrocomp Consulting, Linlithgow, Scotland. Steve Cumella of Bill Barrett Corp in Denver, CO gave permission to use the Fig 5 gas well productivity data. Matlab 2D finite difference acoustic wave propagation code was supplied by Heiner Igel, Technical University of Munich. Fluid pressure computation for heterogeneous media was performed with the Matlab PDE Toolbox. Matlab singular value decomposition and other matrix algorithms were used for travel-time inversion. The Matlab academic licence is held by Andrew Curtis, University of Edinburgh. We are grateful to these colleagues for their cooperation.

References

Barkved, O. and Kristiansen, T. [2005] Seismic time-lapse effects and stress changes: Examples from a compacting reservoir. *The Leading Edge*, **24**, 1244-1248.

Binney, J.J., Dowrick, N.J., Fisher, A.J., and Newman, M.E.J. [1995] *The Theory of Critical Phenomena*. Clarendon Press, Oxford.

Eiken, O. and Tondel, R. [2005] Sensitivity of time-lapse seismic data to pore pressure changes: is quantification possible? *The Leading Edge*, **24**, 1250-1254.

Hofmann, R., Xu, X.X, Batzle, M., Prasad, M., Furre, A.K., and Pillitteri, A. [2005] Effective pressure or what is the effect of pressure. *The Leading Edge*, **24**, 1256-1260.

Goff, J.A. and Holliger, K. (Eds.) [2002] *Heterogeneity of the Crust and Upper Mantle – Nature, Scaling and Seismic Properties*. Kluwer Academic/Plenum Publishers, New York.

Landro, M., Digranes, P., and Stronen, L. K. [2005] Pressure depletion measured by time-lapse VSP. *The Leading Edge*, **24**, 1226-1232.

Leary, P.C. [1997] Rock as critical-point system and the inherent implausibility of reliable earthquake prediction. *Geophysical Journal International,* **131**, 451-466.

Leary, P.C. [2002] In: J.A. Goff & K. Holliger (Eds.) *Heterogeneity of the Crust and Upper Mantle - Nature, Scaling and Seismic Properties,* Kluwer Academic/Plenum Publishers, New York, 155-186.

Leary, P.C. and Al-Kindy, F. [2002] Power-law scaling of spatially correlated porosity and log(permeability) sequences from north-central North Sea Brae oilfield well core. *Geophysical Journal International,* **148**, 426-442.

Leary, P.C. and Walter, L.A. [2005a] Physical model for the downhole orbital vibrator (DOV) - I. Acoustic and borehole seismic radiation. *Geophysical Journal International,* 163, 647–662.

Leary, P.C. and Walter, L.A. [2005b] Physical model for the downhole orbital vibrator (DOV) - II. Rotary correlation wavelets and time-lapse seismics. *Geophysical Journal International,* **163**, 663–688.

Leary, P.C., Ayres, W., Yang, W.J., and Chang, X.F. [2005] Crosswell seismic waveguide phenomenology of reservoir sands & shales at offsets >600 m, Liaohe Oil Field, NE China. *Geophysical Journal International,* **163**, 285–307.

Stauffer, D. and Aharony, A. [1994] *Introduction to Percolation Theory*. Taylor & Francis, London.